Towards RGB Photoelasticity: Full-field Automated Photoelasticity in White Light

by A. Ajovalasit, S. Barone and G. Petrucci

ABSTRACT—In this paper a new full-field method for the automatic analysis of isochromatic fringes in white light is presented. The method, named RGB photoelasticity, eliminates the typical drawbacks of the classical approach to photoelasticity in white light which requires a subjective analysis of colors and an experienced analyst to acquire and interpret the results.

The proposed method makes it possible to determine retardations uniquely in the range of 0–3 fringe orders. For this purpose the isochromatics are acquired by means of a color video camera and the colors are decomposed in the three primary colors (red, green and blue) and compared to those stored in a calibration array in the system. Furthermore, the influence of various spurious effects on the accuracy of the proposed method is experimentally evaluated.

Introduction

Various digital-image-processing techniques have been recently applied to the optical methods of experimental mechanics and, in particular, to photoelasticity. Using monochromatic light, the analysis of isochromatics can be performed by:

(1) methods based on extraction of fringe centers[1–8]
(2) methods as half-fringe photoelasticity (HFP)[9–13]
(3) methods based on phase stepping[14–18]
(4) heterodyne methods[19]
(5) methods based on Fourier and Hilbert transforms[20–21]

Furthermore, photoelasticity makes it possible to use white light. For example, the use of white light is well known for analysis of isochromatic fringes in birefringent coatings and for nondestructive evaluation of residual stresses in glass and plastics.

Using white light, the fringe order has been determined automatically by point-by-point methods based on a spectrophotometer setup measuring the spectral content of light emerging from a polariscope.[22–29] These methods, named SCA (spectral content analysis), can also uniquely evaluate high retardations, but by point-by-point measurements. However, a modification to a full-field method has been recently proposed,[30] based on the use of eight images obtained by eight narrow-band filters.

A. Ajovalasit (SEM Member) is Professor, S. Barone is PhD Student, and G. Petrucci is Graduate Technician, Department of Mechanics and Aeronautics, Universita degli Studi, Viale delle Scienze, 90128 Palermo, Italy.

Original manuscript submitted: December 23, 1993. Final manuscript received: October 27, 1994.

This paper describes the automatic analysis of full-field isochromatics obtained in white light using a color digital-image-processing system. In particular the system, already proposed by the authors,[31–33] is further developed to consider the influence of several spurious effects. The proposed method is a full-field procedure, such as the HFP technique, but it makes it possible to fully determine up to three fringe orders.

Acquisition in White Light

Equation of the Polariscope

Using monochromatic light of wavelength λ_0, the intensities emerging from dark- and light-field circular polariscopes can be represented respectively as

$$I = I_0 \sin^2 \frac{\pi\Delta}{\lambda_0} \quad \text{(dark field)} \tag{1}$$

$$I = I_0 \cos^2 \frac{\pi\Delta}{\lambda_0} \quad \text{(light field)} \tag{2}$$

where, for the plane-stress state, the relation between the retardation Δ and the principal stress difference $(\sigma_1 - \sigma_2)$ is

$$\Delta = C_0 d(\sigma_1 - \sigma_2) \tag{3}$$

where d is the specimen thickness and C_0 is the stress-optic coefficient at wavelength λ_0. Using a light source of wavelength λ_0, the relative retardation δ is

$$\delta = \frac{\Delta}{\lambda_0} = N \pm \delta^* \quad (N = 0, 1, 2, \ldots; \quad \delta^* \leq 0, 5) \tag{4}$$

Therefore eq (1), referring to the dark-field polariscope, becomes

$$I = I_0 \sin^2(\pi N \pm \delta^*) = I_0 \sin^2\delta^* \tag{5}$$

Equation (5) indicates that only the fractional part δ^* can be found by measurements of the intensity of light, while the integer order N is lost. In techniques like the HFP[9–10] using monochromatic light, the maximum evaluable retardation is therefore limited to 0.5 fringe orders. The use of more wavelengths of light or of the full visible spectrum allows the determination of the complete retardation δ.

Using white light and taking into account the dispersion of birefringence and the error of quarter wave plates, the equation of the dark-field polariscope (1) with crossed optical retarders becomes[24–26]

$$I = \frac{1}{\lambda_2 - \lambda_1} \int_{\lambda_1}^{\lambda_2} I_0(\lambda) \sin^2 \left(\frac{\pi \Delta}{\lambda} \frac{C_\lambda}{C_0} \right) (1 - \cos^2 2\alpha \sin^2 \varepsilon) d\lambda \quad (6)$$

whereas, the equation of the light-field circular polariscope (2) with crossed optical retarders is[33]

$$I = \frac{1}{\lambda_2 - \lambda_1} \int_{\lambda_1}^{\lambda_2} I_0(\lambda) \left[\cos^2 \left(\frac{\pi \Delta}{\lambda} \frac{C_\lambda}{C_0} \right) (1 - \cos^2 2\alpha \sin^2 \varepsilon) + \cos^2 2\alpha \sin^2 \varepsilon \right] d\lambda \quad (7)$$

where

λ_1 and λ_2 = the lower and upper limits of the spectrum of the light source used

C_λ/C_0 = the term which accounts for the dispersion of birefringence, being C_λ and C_0 the stress-optic coefficients at arbitrary wavelength λ and at the reference wavelength λ_0, respectively

α = the isoclinic angle, i.e., the angle between the direction of σ_1 and the reference axis

ε = the error of the retardation of the quarter wave plates given by

$$\varepsilon = \frac{\pi}{2} \left(\frac{\lambda_0}{\lambda} - 1 \right) \quad (8)$$

where λ_0 is the matching wavelength of the quarter wave plates and λ is the generic wavelength. $\cos^2\alpha \sin^2 2\varepsilon$ is the term which accounts for the error ε.

The previous relations indicate that the influence of optical retarders in a dark field is different from that in a light field. In particular, the retardation error ε produces an attenuation of the maximum intensities in a dark field and an increase of the minimum intensities in a light field.

In accordance with eqs (6) and (7), the isochromatics are colored because the attenuation and the extinction depend on the wavelengths λ of the spectrum of the light source. Table 1 shows a typical progression of colors observed using a dark-field circular polariscope in white light. With increasing retardation, overlapping between extinctions occurs more frequently and the intensity of the observed colors begins to fade. Tables of this kind (Ref. 10, p. 215) make it possible to determine retardations on the basis of colors with an accuracy of about 0.2 fringe orders.

Acquisition by a Color Video Camera

The digital-image-processing system is composed of (Fig. 1):

(1) a color video camera with an independent sensor CCD for each of the red, green and blue colors, which are defined primary colors;[34]

(2) a 16-bit digital board with resolution of 512 × 512 pixels capable of assigning 5 bits to each of the three primary colors corresponding to 32 intensity levels;

(3) a personal computer with a 486 processor at 25 MHz;

(4) an analog monitor.

A stressed photoelastic model is placed in a dark field polariscope, with crossed quarter wave plates corrected for yellow light (λ_0 = 590 nm).

The isochromatic fringes are acquired in white light by the video camera and the colors are decomposed in the three primary colors. The board digitizes the primary colors, red, green and blue in three intensity levels, in the following denoted by the R, G and B symbols respectively. In Table 1 the typical R, G and B levels corresponding to the first four orders are shown.

TABLE 1—DARK-FIELD CIRCULAR POLARISCOPE IN WHITE LIGHT: OBSERVED COLORS (1), CORRESPONDING RETARDATIONS (2)–(3) AND R, G, B LEVELS (4)–(6)

(1) Observed Colors	(2) Retardation Δ (nm)	(3) Relative Retardation $\delta = \Delta/\lambda_0$ λ_0 = 590	(4) R	(5) G	(6) (B)
black	0	0	5	4	5
gray	50	0.09	8	10	12
white	200	0.34	25	26	28
yellow	400	0.68	25	19	10
orange	450	0.76	22	13	6
red	500	0.85	16	6	12
tint of passage 1	590	1.00	7	11	24
blue	650	1.10	8	19	28
green	700	1.19	13	23	27
yellow	800	1.36	24	27	19
orange	900	1.53	28	22	8
red	1000	1.70	26	13	18
tint of passage 2	1180	2.00	11	18	26
green	1300	2.20	12	25	16
yellow	1400	2.37	21	24	12
pink-red	1550	2.63	27	14	24
tint of passage 3	1770	3.00	16	20	18
pale green	1800	3.05	14	22	16
pink	2100	3.56	25	18	19
tint of passage 4	2360	4.00	16	20	23
pale green	2500	4.24	19	19	21

The R, G and B levels depend on the spectrum of the light source and on the setup of the acquisition system.

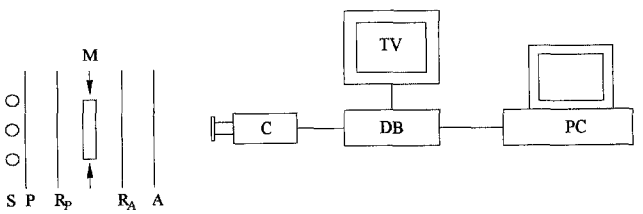

Fig. 1—Experimental setup (A, P = polarizers; M = model; Rp, R_A = optical retarders; S = light source; PC = personal computer; DB = digital board; C = RGB camera; TV = monitor TV)

Using white light with a dark-field circular polariscope and taking into account the relationship in eq (6), the equations of the intensities emerging from the RGB filters of the camera can be written as

$$I_i = \frac{1}{\lambda_{i2} - \lambda_{i1}} \int_{\lambda_{i1}}^{\lambda_{i2}} F_i(\lambda) I_0(\lambda) \cdot \sin^2 \left(\frac{\pi \Delta}{\lambda} \frac{C_\lambda}{C_0} \right) (1 - \cos^2 2\alpha \sin^2 \varepsilon) d\lambda \quad (i = r, g, b) \quad (9)$$

whereas, using a light-field circular polariscope and taking into account the relationship in eq (7), the equations of the intensities can be written as

$$I_i = \frac{1}{\lambda_{i2} - \lambda_{i1}} \int_{\lambda_{i1}}^{\lambda_{i2}} F_i(\lambda) I_0(\lambda) \cdot \left[\cos^2 \left(\frac{\pi \Delta}{\lambda} \frac{C_\lambda}{C_0} \right) (1 - \cos^2 2\alpha \sin^2 \varepsilon) + \cos^2 2\alpha \sin^2 \varepsilon \right] d\lambda \quad (i = r, g, b) \tag{10}$$

where λ_{i1} and λ_{i2} are the lower and upper limits of the spectrum as it is acquired by the filter i, and F_i ($i = r, g, b$) are the spectral responses of the red, green and blue filters of the camera.

Figure 2 shows a typical plot of R, G and B levels as functions of retardation δ. Because of the well-known attenuation of the isochromatic fringes in white light, the variations of R, G and B signals begin to fade for retardations higher than 4–5 orders. For lower orders, using eqs (9) and (10) allows us to evaluate the unknown retardation Δ (or δ) by processing of the acquired RGB levels.

Calibration Procedure

The intensity eqs (9) and (10) can be used to evaluate Δ only if the F_i functions, the transfer function of the digital board (relationship between the RGB values and intensity values I_r I_g and I_b), the dispersion of birefringence and the isoclinic angle α are known. This procedure is usually applied by point-by-point techniques, such as SCA (spectral content analysis[24–29]). In the proposed method a data-base search approach is applied. In particular the procedure for calibration consists of (1) applying a bending load to a calibration beam [Fig. 3(a)] to produce a maximum relative retardation N_m; (2) acquiring the RGB values [Fig. 4(a)] at each pixel (index i) along a transverse line on the calibration beam and storing them in an array with index i growing with retardation.

If the first pixel of the calibration corresponds to a fringe of zero order, the retardation δ_i corresponding to the pixel i is

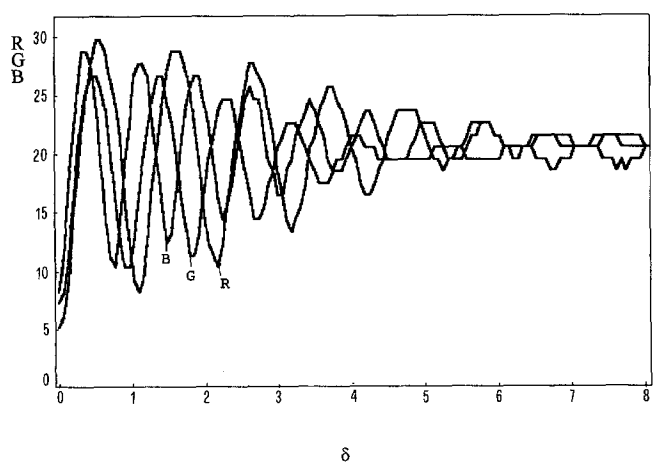

Fig. 2—Typical plot of R, G and B levels as functions of retardation δ

$$\delta_i = N_m \frac{i}{i_m} \tag{11}$$

where i_m is the number of the acquired RGB values calibrating the system.

The R, G and B levels are directly linked with the retardation Δ or δ (obtained in monochromatic light of wavelength λ_0). Therefore, if the calibration specimen and the model are made from the same photoelastic material, the calibration takes into account the dispersion of birefringence.

Equation (11) is valid provided that the retardations δ in the calibration beam are linear. This has been tested by means of the analysis of isochromatics in monochromatic light [Fig. 4(b)]. A deviation of less than 0.01 fringe orders has been evaluated, except at the last point where a deviation of 0.04 orders has been estimated.

The Search of Retardation

During the analysis, the levels R_m, G_m and B_m are measured at pixels in the specimen where the retardation has to be determined. Using the calibration array, the retardation corresponding to each set of R_m, G_m and B_m levels can be evaluated. The general procedure consists of:

(1) comparing the R_m, G_m and B_m values digitized at each point of the specimen with the R_i, G_i and B_i values stored in the calibration table by means of the error function defined as

$$E_i = (R_i - R_m)^2 + (G_i - G_m)^2 + (B_i - B_m)^2 \tag{12}$$

for each index i of the calibration table;

(2) searching the value of the index i that minimizes the error function (12);

(3) evaluating δ_i by means of eq (11).

Due to the attenuation of the RGB levels for retardations higher than 4–5 orders, the maximum measurable retardation is limited to three orders. In this case the retardation search procedure provides exact values with the exception of a few pixels where a measurement error can occur due to similarity of the colors of different orders. To avoid these errors, the proposed method[32] considers the two best results of the search procedure choosing that one better approaching the retardation in the nearest pixels. The search procedure takes about 1 second for 1000 pixels.

Figure 3 shows the isochromatic pattern for the calibration beam [Fig. 3(a)] and of the tested model [Fig. 3(b)] in dark field. Figure 5(a) is a plot of the R_m, G_m and B_m levels along the line A-B drawn on the model of Fig. 3(b). Figure 5(b) shows the results of measurements obtained by the proposed method. In the same figure, the retardations obtained by the classical technique using monochromatic light are also shown. The maximum error between values obtained by the automated method using white light and the classical measurements using monochromatic light is less than 0.02 fringe orders.

Experimental Results

The response of the proposed method to the influence of retardation error of the quarter wave plates, temporal stability and noise, light-intensity variations and fringe gradient is analyzed below.

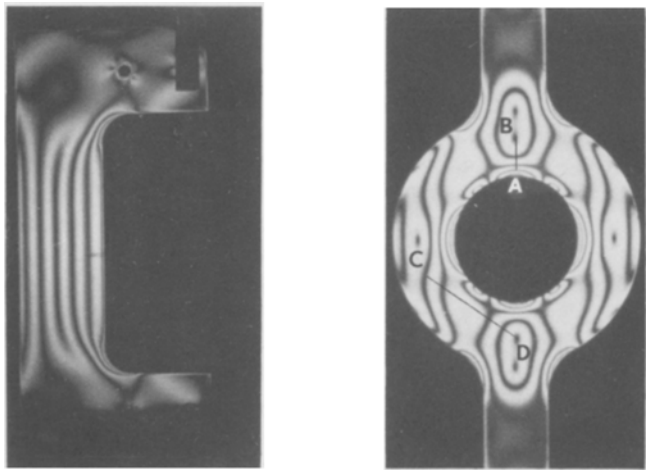

(a) (b)

Fig. 3—Dark-field isochromatic fringe pattern for the calibration beam (a) and for the tested model (b)

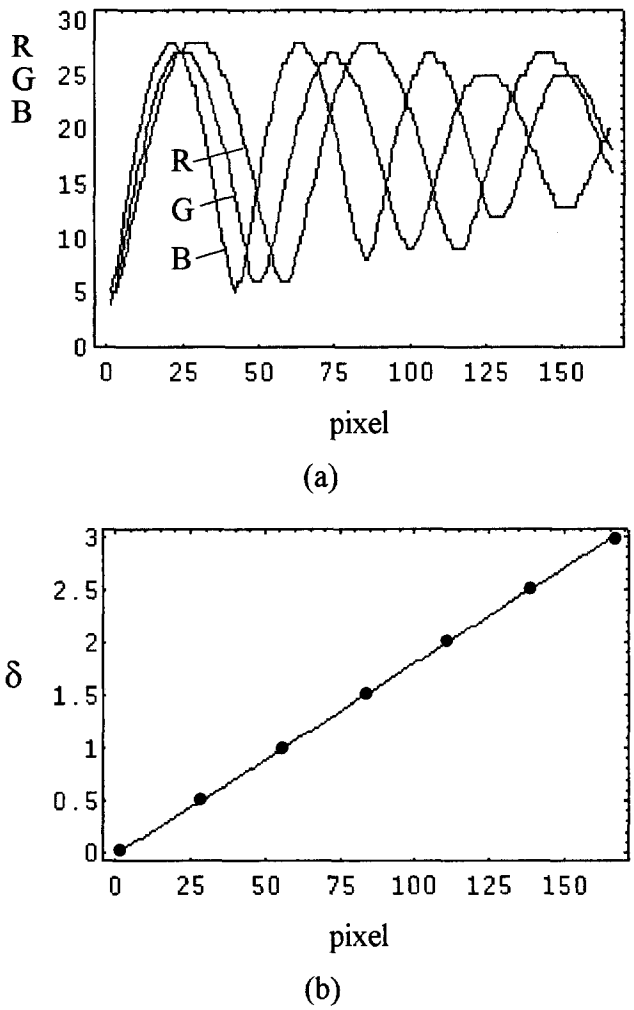

Fig. 4—(a) R, G and B signals along the transverse section of the calibration beam; (b) retardation for the calibration beam obtained by the proposed method (——) with independent experimental points (•)

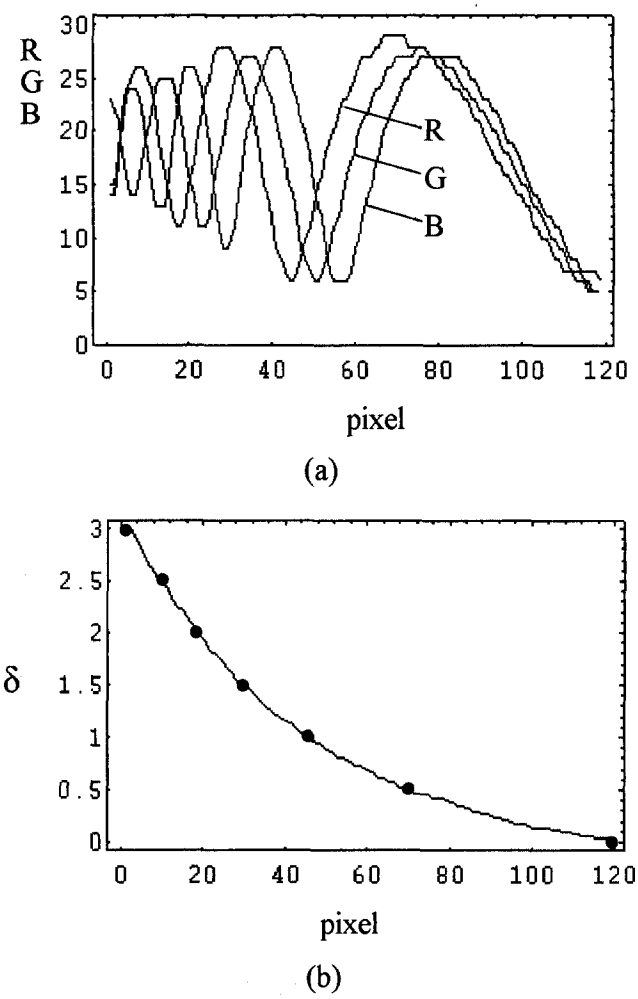

Fig. 5—(a) R_m, G_m and B_m levels measured along the line A-B drawn on the specimen of Fig. 3; (b) corresponding retardations obtained by the proposed method (——) with independent experimental points (•)

Influence of the Retardation Error

The equations of polariscope (9) and (10) show that the influence of errors ε of optical retarders depends on the isoclinic angle α; there is maximum error where α = 0 deg (principal stresses parallel to polarizers), whereas no error occurs where α = 45 deg (principal stresses parallel to retarders).

The analysis of the influence of the retardation error ε was performed in white light using a polariscope with crossed optical retarders corrected for yellow light (λ_0 = 590 nm). A specimen subjected to a bending load was employed both for the calibration of the system and for the retardation measurements. The isochromatics were acquired for α = 0 deg, α = 22.5 deg and α = 45 deg. Figure 6 shows the plots of blue levels along a transverse section of the calibration specimen for α = 0 deg and α = 45 deg, in dark [Fig. 6(a)] and light field [Fig. 6(b)].

According to the theoretical results of eqs (6) and (7), it can be noted, for α = 0 deg, an attenuation of the maximum intensities in dark field and an increase of the minimum intensities in light field. Furthermore, the measurement errors δ′-δ were estimated calibrating for α = 0 deg and measuring for α = 45 deg and calibrating for α = 22.5

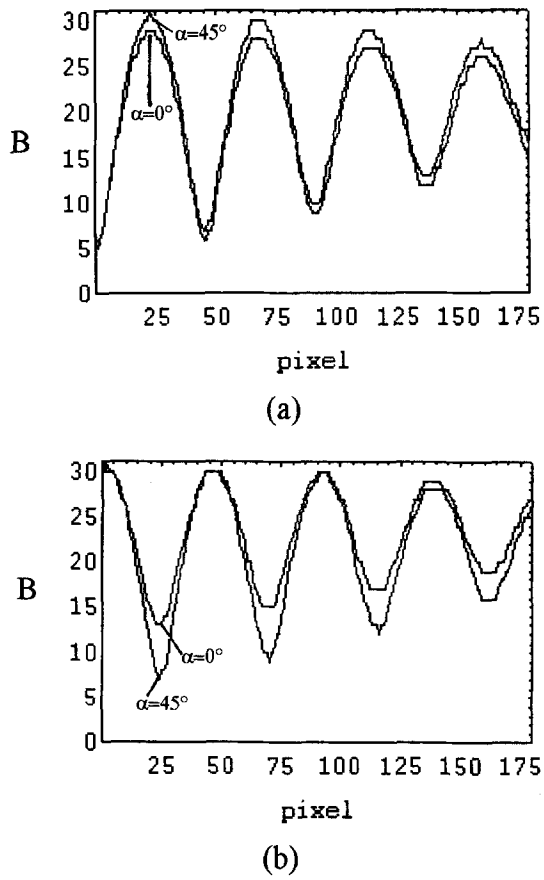

Fig. 6—Influence of the quarter-wave-plates error. Blue intensity levels (B) along a transverse section of the calibration specimen for α = 0 deg and α = 45 deg: (a) in dark field; (b) in light field

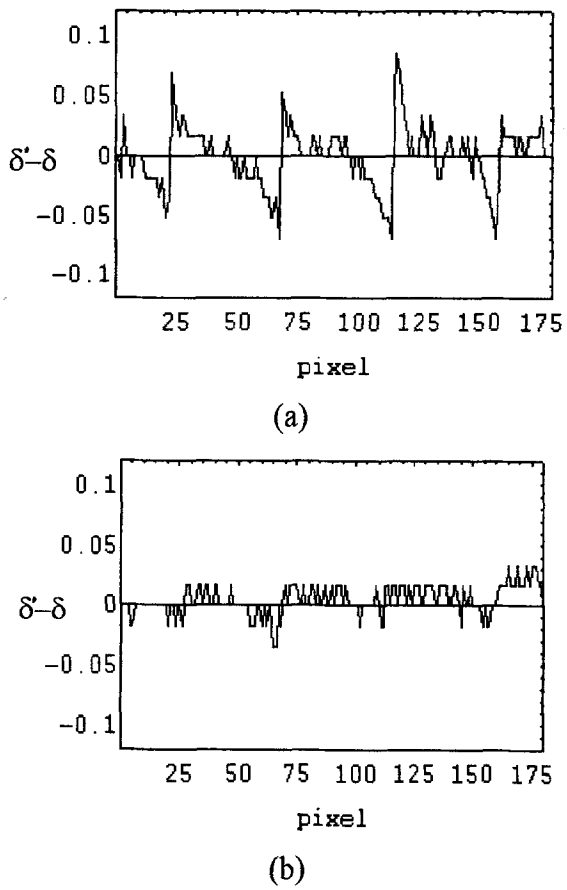

Fig. 7—Influence of the quarter-wave-plates error on the measurement of the retardation. Measured errors δ'-δ in fringe orders: (a) calibration for α = 0 deg and measurements for α = 45 deg; (b) calibration for α = 22.5 deg and measurements for α = 0 deg

deg and measuring for α = 0 deg and for α = 45 deg. The results are shown in Fig. 7 for the light-field polariscope. It can be seen that a considerable decrease in the errors was obtained carrying out the calibration for α = 22.5 deg. Thus, to minimize the influence of optical-retarder error, the calibration is performed with α = 22.5 deg, as proposed by R.V. Baud for a dark field in classical method.[35] The whole analysis, reported in Ref. 33, indicates that the calibration for α = 22.5 deg provides higher improvements in a light field.

Stability and Noise

The temporal stability of the system has been analyzed by performing the calibration at various time intervals. At each time the deviations proved to be not higher than 0.02 fringe orders.

The digitized R, G and B signals are also affected by high frequency random noise due to the electronics. The influence of such noise on retardation measurements is almost negligible. However, the best noise suppression was achieved by a median filter, applied separately to each RGB signal, using a two-dimensional window of square shape (3 × 3 or 5 × 5 pixels).

Sensitivity to Variations of Light Intensity

The spatial and temporal variations of light intensity obviously influence the evaluation of the fringe order. In the proposed method, a procedure to reduce such an influence was developed. For this purpose, each R, G and B level in the calibration beam and in the model can be divided by the corresponding sum R+G+B (normalization).

The accuracy of this procedure was evaluated by performing the calibration in the standard state and measuring the retardation after placing neutral filters with a density of 10, 20 and 30 percent in front of the camera. Figure 8 shows the deviations $\delta' - \delta$ between the retardations evaluated along a transverse section of the calibration beam, without and with attenuation of 20 percent. Similar results were obtained with 10 percent and 30 percent attenuating filters. Neglecting the first part corresponding to retardations lower than 0.5 fringe orders, in the three cases, the error is lower than 0.03 orders. For $\delta < 0.5$ fringe orders the error is higher because the colors corresponding to this range give the same normalized value since they are almost different levels of grey (from black for zero order to white for 0.5 order).

Figure 9 shows the results obtained along the line C-D drawn on the model of Fig. 3(b) performing the calibration without attenuation. In particular Fig. 9(a) shows the R, G and B levels not attenuated, whereas Fig. 9(b) shows the same signals with an attenuation of 30 percent. The retardations, drawn in Fig. 9(c) and 9(d), show a strict correspondence for $\delta > 0.5$ fringe orders.

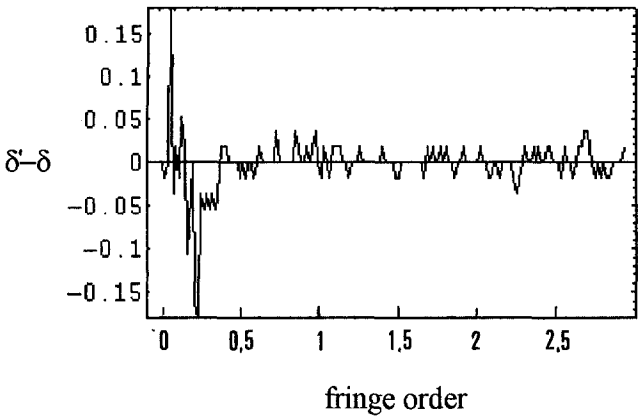

Fig. 8—Influence of 20-percent light attenuation on the evaluation of the retardation

In the polariscope used for this investigation the spatial variation of the light intensity is less than five percent and therefore the error due to the attenuation can be neglected.

Influence of Fringe Gradient

The fringe gradient in the model is usually different from that in the calibration specimen; moreover, this difference can be high at points of stress concentration.

The influence of the fringe gradient has been evaluated performing the calibration with the minimum image gradient achievable by the proposed system (maximum magnification), that is

$$\left(\frac{\Delta N}{\Delta p_x}\right)_{cal} = 0.018 \quad \left[\frac{\text{order}}{\text{pixel}}\right] \tag{13}$$

where ΔN and Δp_x are the increments of fringe orders and corresponding pixels, respectively.

The model has been observed by changing the magnification to obtain image gradients higher than those ones in calibration. The experimental results show that the influence of the fringe gradient is negligible for image gradients less than

$$\left(\frac{\Delta N}{\Delta p_x}\right)_{\max} = 0.1 \quad \left[\frac{\text{order}}{\text{pixel}}\right] \tag{14}$$

If the stress concentration is high, the image must be magnified to make the image fringe gradient not higher than 0.1 order/pixel.

The maximum fringe gradient in the model is

$$\left(\frac{\Delta N}{\Delta l}\right)_{\max} = \frac{1}{k}\left(\frac{\Delta N}{\Delta p_x}\right)_{\max} \quad \left[\frac{\text{order}}{\text{mm}}\right] \tag{15}$$

where

$$l = k \times p_x \tag{16}$$

where l is the length in the model, p_x is the corresponding number of pixels and k (mm/pixel) is the scale factor.

By means of the proposed system, the maximum value of $1/k$ is 9 without an additional lens and 36 with an ad-

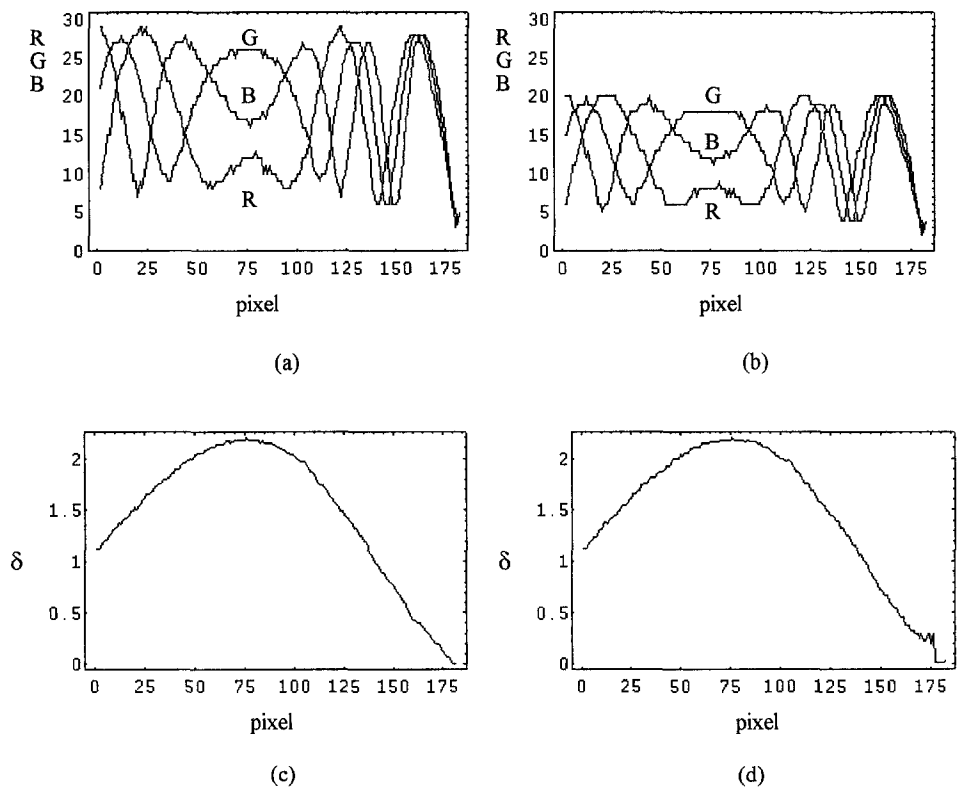

Fig. 9—Influence of light attenuation: R, G and B levels along the line C-D drawn on the model of Fig. 3 and measured retardations: (a)-(c) without attenuation, (b)-(d) 30-percent attenuation

ditional lens. Thus, taking into account eqs (14) and (15), the higher analyzable fringe gradients are 0.9 order/mm and 3.6 order/mm, respectively.

Figure 10 shows the plot of retardations in a region with a fringe gradient of 3.6 order/mm.

Conclusions

This paper presents a new method for full-field stress analysis, named RGB photoelasticity and based on the use of a color video camera. It is shown that by using white light, automatic acquisition of isochromatics makes it possible to evaluate retardations by analyzing the R (red), G (green) and B (blue) levels. For this purpose the system is calibrated by means of a calibration array which can be considered as an evolution of the color tables used by classical photoelasticity in white light.

In particular the proposed method makes it possible: (1) to determine retardations higher than those (0.5 fringe orders) achievable by techniques such as half-fringe photoelasticity: in particular to evaluate uniquely retardations up to three fringe orders; (2) to take into account the dispersion of birefringence in calibrating the system by means of a specimen made from the same photoelastic material of the model; (3) to take into account the error of optical retarders both in a dark field and in a light field.

Three features of this method of experimental analysis are: (1) the temporal stability of this system incurs errors no larger than 0.02 fringe orders; (2) the sensitivity to the light intensity variations (also of 30 percent) is very low; (3) the influence of fringe gradients is negligible until 0.1 order/pixel.

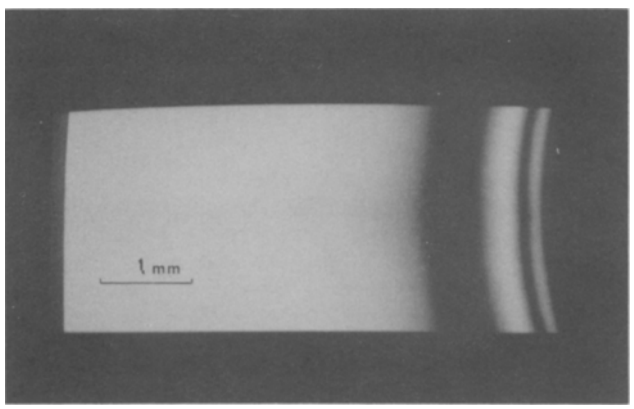

(a)

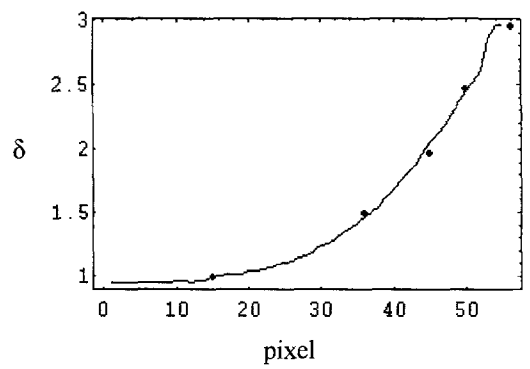

(b)

Fig. 10—Influence of fringe gradient: (a) region of high fringe gradient (3.6 order/mm) in the model; (b) retardations obtained by the proposed method (——) with independent experimental points (•)

Acknowledgments

The research described in this paper has been financed in part by the Italian Council of Research (CNR) through grants 90.00771.CT07 and 93.01010.CT07, and by HURST 60%.

References

1. *Vicentini, V., and Molinar, G.F., "Elaborazione di dati fotoelastici per mezzo di un piccolo calcolatore e plotter," Proc. 1st AIAS Conf. Dept. of Mech. and Aero. Univ. of Palermo, 59–70 (1972).*
2. *Muller, R.K. and Saackel, L.R., "Complete Automatic Analysis of Photoelastic Fringes,"* EXPERIMENTAL MECHANICS, **19** *(7), 245–251 (1979).*
3. *Segugi, Y., Tomita, Y. and Watanabe, M., "Computer-aided Fringe Pattern Analyzer: a Case of Photoelastic Fringes,"* EXPERIMENTAL MECHANICS, **12** *(10), 362–370 (1979).*
4. *Conti, P. and Beghini, M., "Analisi fotoelastica assistita da calcolatore," Proc. 14th AIAS Conf., Institute of Machines, University of Catania, 189–200, (1986).*
5. *Gillies, R.C., Keskin, O., Telfer, D. and Whiteley, K., "An Image Processing Approach to Photoelastic Fringe Patterns," Spie* **814**, *Photomechanics and Speckle Metrology, 58–70 (1987).*
6. *Zhang, F., Su, M.Z. and Chen B., "A Digital Image Processing System for Photoelastic Stress Analysis," Spie* **814**, *Photomechanics and Speckle Metrology, 806–809 (1987).*
7. *Unezaky, E., Tamaki, T. and Takahashi, S., "Automatic Stress Analysis of Photoelastic Experiments by Use of Image Processing,"* EXPERIMENTAL TECHNIQUES, **13** *(12), 22–27 (1989).*
8. *Merloni, R. and Paone, N., "Un sistema per l'elaborazione automatica delle frange fotoelastiche: sviluppo del metodo di misura ed analisi dell'incertezza," Proc. 20th AIAS Conf., Dept. of Mech. and Aero., Univ. of Palermo, 99–108 (1991).*
9. *Voloshin, A.S. and Burger, C.P., "Half Fringe Photoelasticity: a New Approach to Whole-field Stress Analysis,"* EXPERIMENTAL MECHANICS, **23** *(3), 304–313 (1983).*
10. *Handbook on Experimental Mechanics, ed. A.S. Kobayashi, Prentice-Hall Inc. and SEM, Englewood Cliffs, NJ (1987).*
11. *Wang, W.C. and Chen, T.L., "Half-fringe Photoelastic Determination of Opening Mode Stress Intensity Factor for Edge Cracked Strips," Eng. Fract. Mech.,* **32** *(1), 111–122 (1989).*
12. *Brown, G.M. and Sullivan, J.L., "The Computer-aided Holophotoelastic Method,"* EXPERIMENTAL MECHANICS, **30** *(2), 135–144 (1990).*
13. *Pasta, A. and Petrucci, G., "Determinazione del fattore delle intensificazione delle tensioni con la fototermoelasticità assistita," Proc. 20th AIAS Conf., Dept. of Mech. and Aero., Univ. of Palermo, 109–119 (1991).*
14. *Hecker, F.W. and Morche, B., "Computer-aided Measurement of Relative Retardations in Plane Photoelasticity," Experimental Stress Analysis, ed. H. Wieringa, Martinus Nijhoff Publ., 535–542, (1986).*
15. *Kihara, T., "Automatic Whole-field Measurement of Photoelasticity Using Linear Polarized Incident Light," Proc. 9th Int. Conf. on Exp. Mech., Copenhagen* **2**, *821–827 (1990).*
16. *Mawatari, S., Takashi, M., Toyada, Y. and Kunio, T., "A Single Valued Representative Function for Determination of Principal Stress Direction in Photoelastic Analysis," Proc. 9th Int. Conf. on Exp. Mech., Copenhagen,* **5**, *2069–2078 (1990).*
17. *Mawatari, S., Takashi, M., Toyada, Y. and Kunio, T., "A New Method of Computer-aided Fringe Order Determination of Isochromatics in Two Dimensional Photoelasticity," Proc. 9th Int. Conf. on Exp. Mech., Copenhagen,* **5**, *2079–2087 (1990).*
18. *Patterson, E.A. and Wang, Z.F., "Towards Full Field Automated Photoelastic Analysis of Complex Components," Strain* **27**, *(2), 49–56 (1991).*

19. *Alasia, F., Barbato, G., Basile, G. and Mosca, M., "Applicazione di un metodo interferometrico ad eterodina per misure fotoelastiche di elevata sensibilità," Proc. 15th AIAS Conf., Dept. of Mech. and Nuclear Design, Univ. of Pisa, 155–167 (1987).*

20. *Sciammarella, C.A. and Ahmadshahi, M.A., "Detection of Fringe Pattern Information Using a Computer Based Method," Experimental Stress Analysis, ed. H. Wieringa, Martinus Nijhoff Publ., 359–368 (1986).*

21. *Quan, C., Bryanston-Cross, P.J. and Judge, T.R., "Photoelastic Stress Analysis Using Carrier Fringe and FFT Techniques," Optics and Lasers in Eng.,* **18** *(2), 79–108 (1993).*

22. *Redner, A.S., "Photoelastic Measurements by Means of Computer-assisted Spectral Contents Analysis,"* EXPERIMENTAL MECHANICS, **25** *(2), 148–153 (1985).*

23. *Redner, A.S., "Photoelastic measurements of residual stress for NDE," Proc. of Spie,* **814**, *Photomechanics and Speckle Metrology, 16–19 (1984).*

24. *Sanford, R.J. and Iyengar, V., "The Measurement of the Complete Photoelastic Fringe Order Using a Spectral Scanner," Proc. 1985 SEM Spring Conf. on Exp. Mech., 160–168 (1985).*

25. *Sanford, R.J., "On the Range of Accuracy of Spectrally Scanned White Light Photoelasticity," Proc. 1986 SEM Conf. on Exp. Mech., 901–908 (1986).*

26. *Voloshin, A.S. and Redner, A.S., "Automated Measurement of Birefringence: Development and Experimental Evaluation of the Techniques,"* EXPERIMENTAL MECHANICS, **29** *(3), 252–257 (1982).*

27. *Marwitz, Kizler and Schuster, "Improved Efficiency in Photoelastic Coatings. Fast Detection of Fringe Order Using Computer Controlled Spectrometry," Proc. 9th Int. Conf. on Exp. Mech., Copenhagen* **2**, *828–838 (1990).*

28. *Ivanova, L. and Nechev, G., "A Method for Investigation of the Residual Stress in Glasses with Spectral Polariscope," Proc. of 9th Int. Conf. on Exp. Mech., Copenhagen,* **2**, *876–883 (1990).*

29. *Haake, S.J. and Patterson, E.A., "Photoelastic Analysis of Frozen Stressed Specimens Using Spectral-content Analysis,"* EXPERIMENTAL MECHANICS, **32** *(3), 266–272 (1992).*

30. *Haake, S.J. and Patterson, E.A., "Photoelastic Analysis Using a Full Field Spectral Contents Analyser," Int. Conf. on Photoelasticity: New Instrumentation, Materials and Data Processing Techniques, London (1993).*

31. *Ajovalasit, A. and Petrucci, G., "Analisi automatica delle frange fotoelastiche in luce bianca," Proc. 18th AIAS Conf., Institute of Mech. Eng., Univ. of Salerno, 395–407 (1990).*

32. *Petrucci, G., "Un sistema completo per l'elaborazione delle frange fotoelastiche in luce bianca," Proc. 20th AIAS Conf., Dept. of Mech. and Aero., Univ. of Palermo, 121–135 (1991).*

33. *Ajovalasit, A., Barone, S. and Petrucci, G., "Automated Photoelasticity in White Light: Influence of Optical Retarders," Int. Conf. on Photoelasticity: New Instrumentation, Materials and Data Processing Techniques, London (1993), and J. of Strain Analysis,* **30** *(1), 29–34 (1995).*

34. *Pratt, W.K., Digital Image Processing, John Wiley & Sons, New York (1978).*

35. *Baud, R.V., "Contribution to Study of Effect of Elliptical Polarization Upon Energy Transmission," J. Opt. Soc. of Amer.,* **21**, *119–123 (1931).*